CARBON 89 (2015) 308–317

Available at www.sciencedirect.com

ScienceDirect

journal homepage: www.elsevier.com/locate/carbon

Excellent electromagnetic interference shielding and mechanical properties of high loading carbon-nanotubes/polymer composites designed using melt recirculation equipped twin-screw extruder

Pawan Verma [a], Parveen Saini [b], Rajender Singh Malik [a,c], Veena Choudhary [a,*]

[a] Centre for Polymer Science & Engineering, Indian Institute of Technology, New Delhi 110016, India
[b] CSIR-National Physical Laboratory, Dr. K.S. Krishnan Marg, New Delhi 110012, India
[c] Department of Chemistry, Deenbandhu Chhotu Ram University of Science and Technology, Murthal, Sonepat 131039, India

ARTICLE INFO

Article history:
Received 6 January 2015
Accepted 24 March 2015
Available online 28 March 2015

ABSTRACT

This paper describes for the first time a facile, scalable and commercially viable melt blending approach involving use of twin-screw extruder with melt recirculation provision, for uniform dispersion of up to 4.6 vol% multiwall carbon nanotubes (MWCNTs) within polypropylene random copolymer (PPCP). Morphological characterization of PPCP/MWCNT nanoscale composites (NCs) was done using scanning electron microscopy and transmission electron microscopy, which show good dispersion of MWCNTs in the PPCP matrix even at high loadings and confirm the formation of true NCs. The improved dispersion leads to the formation of electrically conducting three dimensional networks of MWCNTs within PPCP matrix at very low percolation threshold (~0.19 vol%). The attainment of dc conductivity value of $\sim 10^{-3}$ S/cm, tensile strength of ~42 MPa and good thermal stability for 4.6 vol% MWCNTs loading NC along with electromagnetic interference (EMI) shielding effectiveness (SE) value of −47 dB (>99.99% attenuation), demonstrate its potential for making light weight, mechanically strong and thermally stable EMI shields. These NCs also display specific SE value of ~−51 dB cm^3/g which is highest among unfoamed polymer NCs.

1. Introduction

The rapid growth of electronics and communication has led to electromagnetic (EM) interference (EMI) as most undesirable by-product [1]. It can be defined as a kind of electronic pollution constituted by conducted and/or radiated EM energy emitted by wide variety of electronic circuits and telecommunication goods, which not only tries to disturb the functioning and performance of electronic appliances but may also adversely affect the health of living organisms. Therefore, a suitable shielding mechanism is required to suppress or eliminate the EM radiation radiated by electronic instruments as well as for the protection of sensitive circuits from external EM emissions [2–4]. It can be achieved by minimizing the influence of incident EM wave by reflection, absorption or multiple-reflection phenomenon. The reflection is regarded as primary mechanism which requires the presence of mobile charge carriers like electrons or holes. In contrast, secondary

* Corresponding author.
E-mail addresses: pksaini@nplindia.org (P. Saini), veenach@hotmail.com, veenac@polymers.iitd.ernet.in (V. Choudhary).
http://dx.doi.org/10.1016/j.carbon.2015.03.063
0008-6223/

mechanism is absorption which depends upon dielectric/magnetic polarization and associated relaxation losses. Metals and their composites are widely employed as EMI shielding materials, but they suffer from disadvantages like high density, processing difficulties, corrosion susceptibility etc. In this consideration, carbon nanotubes (CNTs) with ultra high strength (10–100 GPa) and modulus (~1.0 TPa) values along with exceptional electrical (10^4–10^6 S/cm) and thermal properties (3000–6000 W/mK), have emerged as highly effective conductive nanofiller for making EMI shielding nanoscale composites (NCs) [5–10]. Therefore, in the recent past, a lot of research has been carried out to prepare CNT filled polymer NCs and to understand their shielding mechanism [11–13]. Anju et al. [14,15] demonstrated that poly(trimethylene terephthalate)/multiwall CNTs (MWCNTs) composite containing 4.76 vol% MWCNT loading display EMI shielding effectiveness (SE) of ~23 and ~42 dB in the X and Ku band respectively. Yang et al. [16] studied the EMI shielding behavior of MWCNT/polystyrene (PS) NCs and achieved SE of 20 dB at 7 wt% MWCNT loading. Yuan-Li et al. [17] studied the EMI shielding response of functionalized-MWCNTs/poly(methyl methacrylate) (PMMA) NCs prepared by in-situ and ex-situ routes, and found that SE increases (at any fixed frequency) with CNT loading. Further, in-situ formed NCs give superior SE (~−17 dB at 12 GHz) at comparative loading than ex-situ formed NCs (SE~−10 dB at 12 GHz). Liu et al. [18] studied single wall CNTs (SWCNTs) based polyurethane (PU) NCs and obtained an EMI SE of 17 dB at 20 wt% SWCNT loading in the frequency range of 8.2–12.4 GHz (X-band), whereas Haung et al.[19] attained much higher EMI SE (20–30 dB) at relatively lower loading (15 wt% SWCNT) in epoxy matrix. Saini et al. showed that incorporation of PANI/MWCNT in PS matrix [20,21] lead to improvement of absorption with maximum SE in the range of −23 to −46 dB depending on the chemical composition of PANI/MWCNT filler and shield thickness. It is important to point out that despite acceptable shielding performance, above studies remained a piece of laboratory work, as they have not paid attention to the mechanical properties (especially strength), cost effectiveness (cheap raw material, process economy or energy saving) or time constraints, which are essential requirement of commercially viable shielding materials. In fact, most works deliberately avoided mechanical strength values due to the high filler loading requirement to achieve acceptable shielding performance, as mechanical properties become extremely poor (even less than matrix) at such high loadings (caused by agglomeration tendency of nanofillers and their non uniform dispersion) [22–25], making the material practically unusable. Interestingly, several attempts have also been made to form high CNT filled (up to 10 wt%) polypropylene (PP) matrix based EMI shielding composites [26–29], due to low cost, chemical inertness, facile processing via melt blending and good mechanical properties of PP. However, again the mechanical properties were not attended, probably due to inherent inferior strength at such high CNTs loading. Recently, twin screw extruder and Banbury mixer are widely employed at lab scale to improve the CNT dispersion inside thermoplastic matrices [30–32]. However, their commercial viability is still low due to time and energy issues arising due to batch operation and shear/residence time limitations. Particularly, in conventional twin screw extruder, the filler dispersion is a function of shear rate (regulate the kneading) and residence time (regulate the overall mixing and stability), both being decided by screw rpm. Due to limited length of screws, any attempt to improve mixing by increasing rpm (shear) result in decrease of residence time thereby decreasing dispersion (as melt get insufficient kneading time). Similarly, any improvement in residence time by decreasing rpm, result in decreased kneading and flow issues, again leading to poor dispersion. A possibility to overcome above problems is to process the material at moderate rpm and reprocess the previously extruded and granulated material through the extruder several times. However, the process becomes commercial unviable due to batch operation with associated time constraint, energy inefficiency and economic unfeasibility. In this context, twin screw extruder with provision for melt recirculation is expected to act as commercially viable processing option for achieving uniform dispersion of high CNT loading inside polymer matrices, simultaneously overcoming the shear/residence time and energy constraints. The melt recirculation option allows effective mixing/dispersion by repeated passes of the polymer melt/filler mixture through the extruder, before being discharged out and extruded.

This article present first report on the successful realization of uniform dispersion of up to 4.6 vol% MWCNTs in PP copolymer (PPCP) matrix via a continuous melt processing technique using twin screw extruder with melt recirculation mechanism. The use of PPCP (in place of PP) also offer processing and economic advantage, due to comparative cost, improved mechanical properties and low (20–30 °C less) processing temperature (energetically economical) compared to PP alongwith better compatibility with fillers. The above combination of PPCP matrix, high CNT loading and processing technique bring commercial viability element into the system that was missing in the previous works. Different NCs were prepared by variation of CNT loading and effect of MWCNTs content on the electrical conductivity, mechanical/thermal properties and EMI shielding response is systematically investigated. The extent of dispersion of MWCNT in the PPCP matrix was investigated using Raman spectroscopy, scanning electron microscopy (SEM) and transmission electron microscopy (TEM) while the effect of MWCNTs content on electrical conductivity (σ), thermal stability and mechanical properties of the PPCP/MWCNT NCs was also measured. The EMI shielding property of these NCs was measured in the frequency range of 12.4–18 GHz (Ku-band). The shielding mechanism of PPCP/MWCNT NCs was studied by quantifying the contribution of absorption and reflection loss to the total EMI SE and considering theoretical aspects of shielding. In addition to shielding response, mechanical and thermal properties of such highly filled NCs have also been presented. The importance of selected processing technique, matrix material and filler combination has been highlighted to demonstrate the practical utility and commercial viability.

2. Experimental

2.1. Materials

PPCP (RepolR120MK from Reliance Industries Limited) with ethylene content of 3–3.5% w/w and having melt flow index of 12 g/10 min (230 °C/2.16 kg) was used as matrix. Multiwall carbon nanotubes (MWCNTs, inner diameter ~ 10–12 nm, outer diameter ~ 30–40 nm and length ~ 20–30 μm) were synthesized by chemical vapor deposition (CVD) of toluene in the presence of ferrocene catalyst [20,33]. Purity of MWCNT determined from thermogravimetric analysis (TGA) was ~95%.

2.2. Preparation of NCs

PPCP/MWCNT NCs were prepared by melt blending technique using co-rotating micro compounder (Model: HAAKE MiniLab II) at processing temperature of 200 °C, mixing time of 10 min and screw speed of 50 rpm. Before blending, MWCNTs and PPCP were oven dried at 110 °C (for 24 h) and 80 °C (for 6 h) respectively, to remove the adsorbed moisture. The extruder was equipped with provision for melt recirculation so that effective mixing can be realized by increasing the number of passes through the extruder. In a typical processing operation, premixed containing a calculated amount of MWCNT powder and PPC granules is charged into the extruder and after the residence time of 10 min, the recirculating melt is diverted toward micro injection molding unit for the preparation of tensile test specimens (Fig. 1). The samples for EMI shielding were formed by compressions molding of granulated form of extruded composite strands. Different compositions were prepared by varying the proportion of MWCNTs and designated as PPCP-0, PPCP-0.2, PPCP-0.4, PPCP-0.9, PPCP-1.8 and PPCP-4.6, where the numeric value indicates the MWCNT loading level in vol%.

2.3. Characterization

Morphology of PPCP/MWCNT NCs was investigated using SEM (EVO-50) and TEM (JEOL 2100F) operating at accelerating voltage of 20 and 200 kV respectively. For SEM studies, manually fractured, gold-coated samples were used whereas for TEM studies, ultra-thin sections (30–80 nm thick) of NCs were prepared using Leica Ultramicrotome. Raman spectrometer (Renishaw InVia Raman microscope) was used to evaluate the structure of PPCP and PPCP/MWCNT NCs. For Raman studies, injection molded samples were used and spectra were recorded using diode laser at 785 nm excitation with Raman shift between 1000 and 1800 cm^{-1}.

The dc electrical conductivity of PPCP/MWCNT NCs was determined using van der Pauw geometry (two-probe contact method) on Keithley semiconductor characterization system (SCS 4200). For this purpose, circular disk shaped samples having diameter 7 mm and thickness 2 mm were cut out from the injection molded samples.

The EMI shielding measurements were performed on Agilent E8362B Vector Network Analyzer (VNA) in the microwave frequency range of 12.4–18 GHz (Ku-band). Rectangular samples (2 mm thick) were inserted in copper sample holder connected between the wave-guide flanges of network analyzer. Full two-port calibration was performed along with the sample holder to neglect any loss and power redistribution due to sample holder. From the measurement of S-parameters, the absorption coefficient and the shielding efficiency of the material were calculated.

The tensile properties were measured on Zwick Universal Tester Model-Z010 at room temperature. The samples were tested in accordance with ASTM D638 Type V test procedure at a crosshead speed of 10 mm/min and gauge length of 7.62 mm.

Thermal stability of the NCs was examined using TGA. Thermogravimetric (TG)/derivative thermogravimetric (DTG)

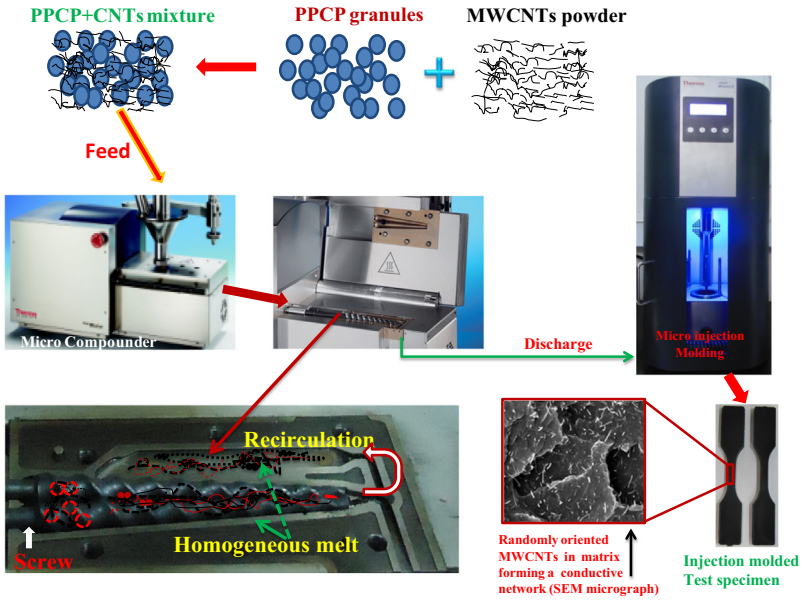

Fig. 1 – Schematic diagram for the fabrication of NCs. (A color version of this figure can be viewed online.)

trace traces were recorded using Perkin Elmer Pyris 6 TGA. For recording (TG)/(DTG) trace, a heating rate of 20 °C/min and a sample size of 8 ± 1 mg were used in N_2 atmosphere (flow rate 60 mL/min).

3. Results and discussion

3.1. *Surface morphology using SEM and TEM*

Fig. 2a, b, c and d shows the SEM micrographs of fractured surfaces of PPCP/MWCNT NCs having 0.2, 0.4, 1.8 and 4.6 vol% MWCNTs respectively whereas Fig. 2e, f, g and h displays the corresponding TEM micrographs. It can be clearly seen in the SEM images that the individual MWCNTs are uniformly dispersed in PPCP matrix with very few entangled (rope like) regions, implying that molten phase mixing inside a twin screw extruder having melt recirculation provision, is an effective way to realize uniform dispersion of MWCNTs and to check their agglomeration inside the host matrix. It is important to point out that uniform mixing and dispersion (even down to nanoscale level) indicate the formation of true nanoscale-composites. Further, their abundance increases with the increase in loading level such that only few unconnected links are present at low MWCNT content (Fig. 2e) whereas at 0.4 vol%, the MWCNTs are found to be randomly oriented and form interconnecting conducting networks (Fig. 2f), suggesting that percolation must be at less than 0.4 vol% loading. The formation of above network at very low MWCNT concentration, reflect the low percolation threshold value, which demonstrate the superiority of micro compounding melt mixing method. Further, the low percolation is expected to manifest itself in terms of minimum disturbance of physico-mechanical properties of PPCP matrix. Consequently, improved mechanical properties are expected to provide a load bearing MWCNT/PPCP interface. In addition, MWCNT being conducting filler, these NCs are also expected to display electrical properties and electromagnetic radiation shielding ability. The TEM images of NCs also display

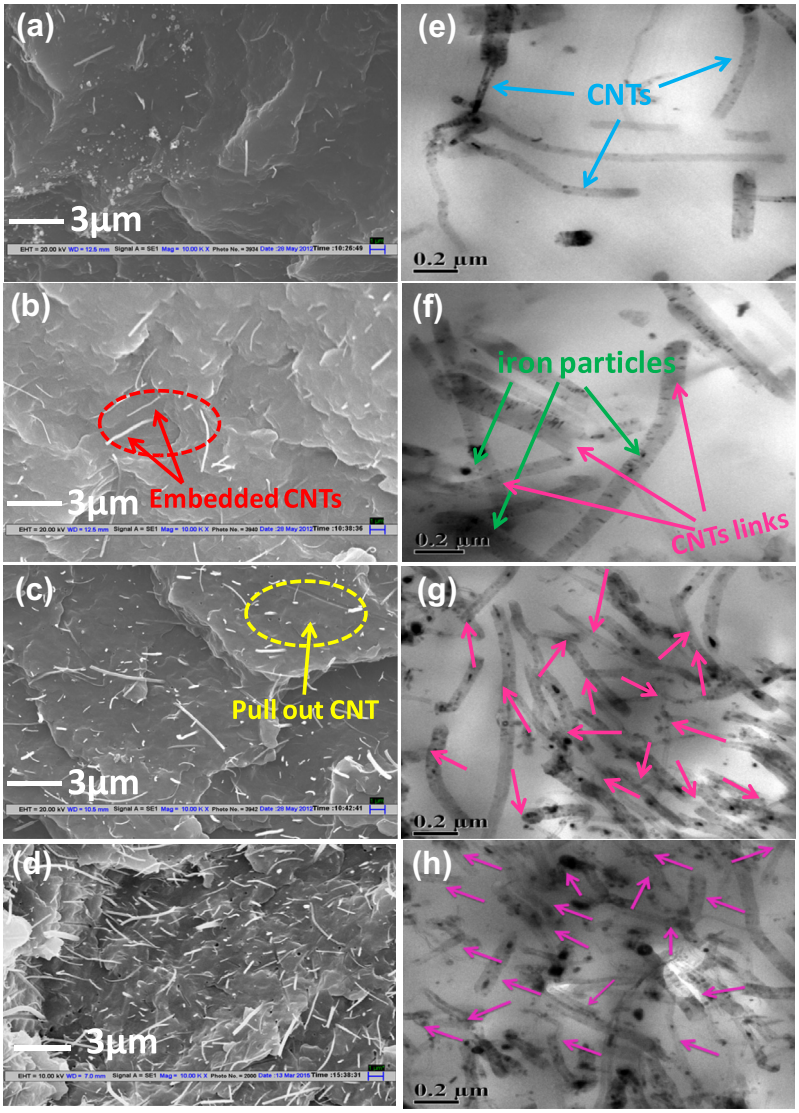

Fig. 2 – SEM & TEM micrographs of PPCP/MWCNT composites: PPCP-0.2 (a and e), PPCP-0.4 (b and f), PPCP-1.8 (c and g) and PPCP-4.6 (d and h). (A color version of this figure can be viewed online.)

presence of iron catalyst inside MWCNT's internal cavity. As the ferromagnetic properties of iron filled CNTs are well established [20,34], therefore; it is expected that these NCs will display additional magnetic losses and improved EMI shielding performance.

3.2. Raman spectroscopy of NCs

Raman spectroscopy is widely employed for the understanding of defect structure or electronic properties of MWCNTs, to get a qualitative idea about degree of graphitization and to assess levels of interactions in NCs. Particularly, the peak position and peak-width of Raman active vibrations are sensitive toward presence of defects, molecular stresses and interaction between different phases.

Raman spectra of MWCNTs/PPCP NCs (Fig. 3) display the superposed signatures of PPCP and MWCNTs. It can be seen that the Raman signatures of the PPCP matrix are rapidly broadened and weaken as the concentration of filler is increased. This can be attributed to the dephasing of the local motions of PPCP chains due to the interactions with the individual MWCNTs. The characteristic "D" and "G" bands of MWCNTs are also observed in NCs samples. The D-band is related to the sp^3 state of carbon and can be used as a proof of disruption of the aromatic π-electrons (sp^2 hybridized) of CNTs i.e. presence of defects. In contrast, G band is related to the graphitic structure (sp^2 carbons). Their position and relative intensity can provide qualitative estimate of interactions and disorder in the system. The careful examination of Raman spectra of NCs also revealed that, as the concentration of MWCNTs increases, the position of D-band show a gradual shift toward lower wave numbers (i.e. 1313 cm^{-1} for PPCP-0.4 to 1308 cm^{-1} for PPCP-4.6), which point toward local stresses and interactions between MWCNTs & PPCP matrix [35,36]. Further, in case of composites, systematic variation of I_D/I_G ratio was also observed i.e. $I_D/I_G \sim 0.79$ for PPCP-0.4 and 0.84 for PPCP-4.6, which reflect processing induced disorder. This can be attributed to the combined effect of generation of defects over MWCNT's outer wall (during elevated temperature and high shearing conditions encountered during melt processing) and active contribution of PPCP matrix. It is important to note that the formed defects create roughness over CNT's surface which may act as anchoring and interfacial interaction sites for the PPCP matrix. Therefore, they may contribute toward stress transfer and expected to improve mechanical properties.

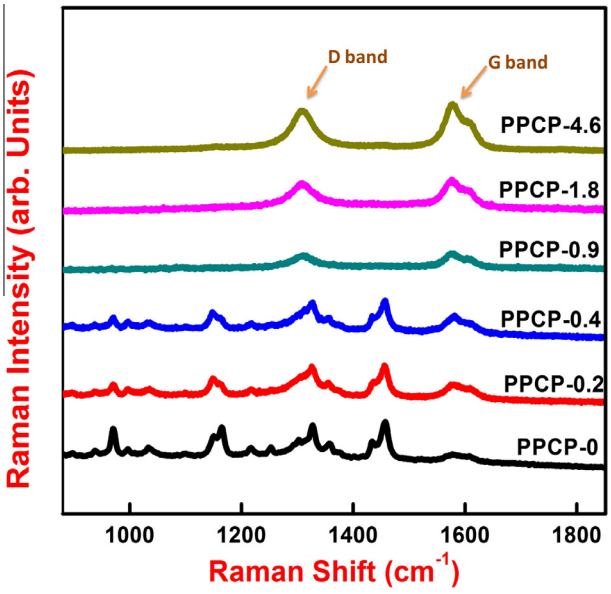

Fig. 3 – Raman spectra of PPCP/MWCNTs composites. (A color version of this figure can be viewed online.)

3.3. Electrical conductivity of PPCP/MWCNT NCs

Fig. 4 shows the dc conductivity (σ) of PPCP/MWCNT NCs as a function of MWCNTs vol% whereas the inset shows the log–log plot of σ versus volume fraction of filler (υ). It can be seen that σ of NCs increases with increasing MWCNT content and display a sharp rise around 0.2 vol% MWCNT loading, suggesting the onset of percolation i.e. formation of a 3D electrically conducting network within PPCP matrix. In the present case, percolation threshold (the minimum filler loading where first continuous network of filler particles was formed within matrix polymer) has been calculated by plotting the electrical conductivity as a function of the reduced volume fraction of MWCNTs and performing data fitting with a power law function [1,6,13,28].

$$\sigma = \sigma_o(\upsilon - \upsilon_c)^{\beta} \quad (1)$$

where σ is the electrical conductivity of the composite, σ_o is characteristic conductivity, υ is the volume fraction of filler, υ_c is volume fraction at the percolation threshold and β is the critical exponent which is related to the system dimensionality. It can be seen (inset Fig. 4) that the slope, (i.e. the critical exponent β) changes from 10.74 to 2.28 at ~0.19 vol% MWCNT loading (marked by the intersection of straight line fits corresponding to these β values), that shows that percolation threshold lies at $\upsilon_c \sim 0.0019$ [37–39]. The occurrence of percolation threshold at such a low MWCNT loading is a direct consequence of processing (inside melt recirculation

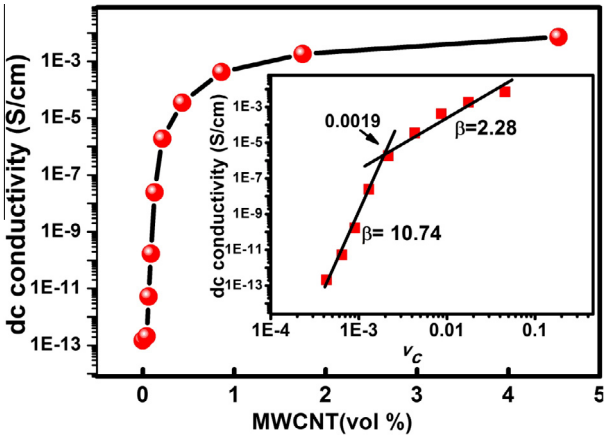

Fig. 4 – Plot of electrical conductivity (σ) versus MWCNT (vol%) for PPCP/MWCNTs composites. Inset shows the log–log plot of σ as a function of (υ_c). (A color version of this figure can be viewed online.)

twin-screw extruder) aided efficient distribution and dispersion of CNTs within PPCP matrix that was also complemented by morphological (SEM/TEM) investigations [40–44]. It is important to point out that PPCP-4.6 display conductivity value of 7.2×10^{-3} S/cm which is near the microwave shielding range and good EMI shielding properties are expected.

3.4. *Shielding effectiveness and shielding mechanism of PPCP/MWCNT NCs*

The EMI SE of a material is the ability to attenuate EM radiation that can be expressed in terms of ratio of incoming (incident) and outgoing (transmitted) power. The EMI attenuation offered by a shield may depend on the three mechanisms: reflection of the wave from the front face of shield, absorption of the wave as it passes through the shield's thickness and multiple reflections of the waves at various interfaces. Therefore, SE of EMI shielding materials is determined by three losses viz. reflection loss (SE_R), absorption loss (SE_A) and multiple reflection losses (SE_M) and can be expressed as [45,46]:

$$SE\ (dB) = (SE_R + SE_A + SE_M) = 10 \log_{10}\left(\frac{P_t}{P_i}\right) = 20 \log_{10}\left(\frac{E_t}{E_i}\right) \quad (2)$$

where P_i (or E_i) and P_t (or E_t) are power of incident and transmitted EM waves respectively. As, the P_t is always less than P_i, therefore, SE is a negative quantity such that a shift toward more negative value means increase in magnitude of SE. It is important to note that the loss associated with multiple reflections can be ignored ($SE_M \sim 0$) when SE_A of EMI shielding material is more than −10 dB (i.e. more negative than −10) so that SE can be expressed as $SE(dB) = SE_R + SE_A$ [16]. Further, it is convenient to express the SE_R and SE_A in the form of reflectance ($R = |S_{11}|^2$) and transmittance ($T = |S_{21}|^2$) as [47]:

$$SE_R = 10 \log (1 - R) \quad (3)$$

$$SE_A = 10 \log [T/(1 - R)] \quad (4)$$

where S_{11} and S_{21} are scattering parameters (S-parameters) measured with the help of VNA.

Fig. 5a shows the frequency dependence of EMI SE of PPCP/MWCNT NCs. It can be seen that, EMI SE of these NCs is almost constant in the entire frequency range, which reflect broadband shielding action. Further, at any fixed frequency, the EMI SE increases with increasing MWCNT content e.g. PPCP-0 display poor EMI shielding response (i.e. SE value of −1 dB that corresponds to more than 79% transmission) whereas SE of −23 dB (>99% attenuation) was obtained only at 1.8% (v/v) MWCNT loading, which further increases to −47.88 dB (that corresponds to blocking of more than 99.99% of the incident EM radiation) for PPCP-4.6. Such a high value of EMI SE at sufficiently low loading can again be attributed to the processing affected good dispersion and distribution of highly conducing (and high aspect ratio) MWCNTs within the PPCP matrix, thereby forming electrically conducing 3D-network. The resolution of SE into reflection and absorption components (Fig. 5b) revealed that though both SE_R and SE_A increases with MWCNT loading, the SE_A increases at much faster rate. It was also observed that although dc conductivity (Fig. 5c) increases exponentially with MWCNT content, the SE increases with much slower rate. It can also be seen that though both conductivity and SE increased with CNT

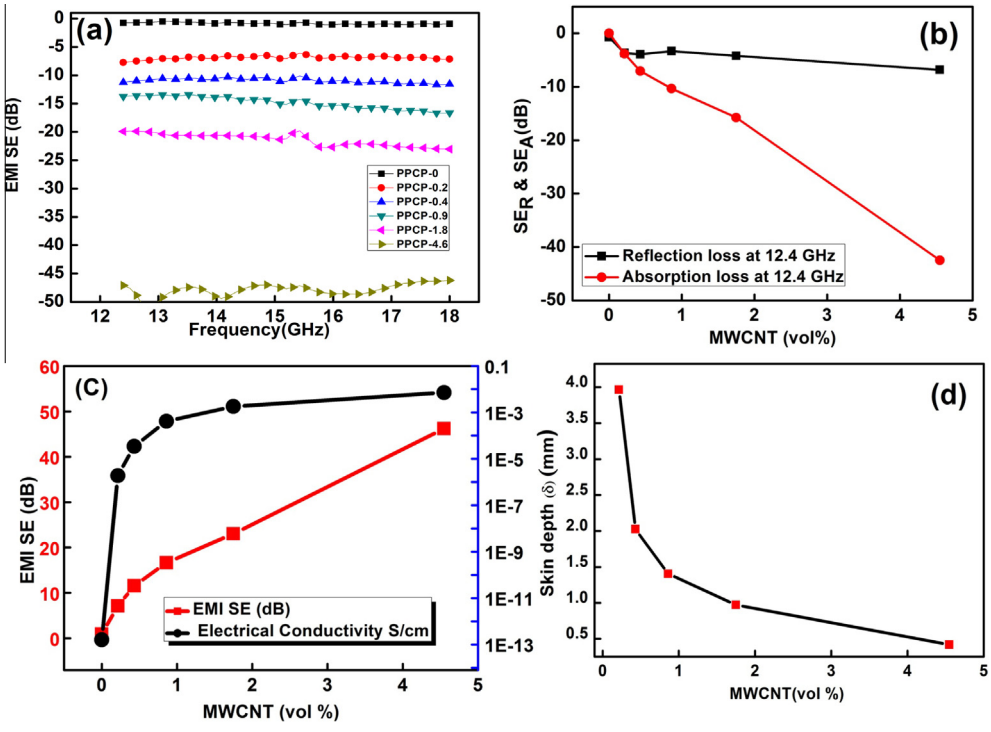

Fig. 5 – (a) Frequency dependence of EMI SE of PPCP/MWCNT composites; variation of (b) SE_R & SE_A, (c) SE & conductivity and (d) skin depth, as a function of MWCNTs content. (A color version of this figure can be viewed online.)

addition, but conductivity did not change significantly after percolation concentration while SE kept on increasing with increasing filler loading (Fig. 5b). It is due to the reason that though both SE and conductivity are related to network formation, the factors affecting SE are more complex than that involved in conduction. As the number of conductive paths increases with the loading of MWCNTs, the EM radiation intercepting regions increases. These regions interact with incident radiation and lead to the higher SE without significantly (not orders or magnitude as near percolation) affecting the conductivity of the material. It is also worth pointing out that incorporation of MWCNTs in PPCP matrix not only leads to establishment and improvement of electrical conductivity but also contribute toward improvement of dielectric properties via interfacial polarization (due to large difference in the electrical conductivity of CNT and PPCP). Such polarization and related relaxation phenomenon also contribute toward improvement of shielding performance via secondary shielding mechanism (i.e. absorption). Further, it should be noted that MWCNTs (formed by CVD) contains entrapped ferromagnetic iron catalyst residues [34] which are also expected to improve the EM energy absorption and dissipation capability [1] resulting in enhancement of microwave shielding effectiveness. As the reflection loss is related to the conductivity of material, the careful comparison (Fig. 5b and c) revealed that the reflection loss follows same pattern as conductivity, i.e. sharp increase at percolation concentration and only moderate increase after that. But, absorption loss showed no significant effect of percolation concentration and display monotonic increase even after percolation. Again, it can be attributed to the fact that, for the conducting NCs, the reflection is mainly governed by conductivity whereas absorption receives contributions from losses due to conduction, interfacial polarization and magnetization. It is important to note that incorporation of MWCNTs also leads to reduction of skin depth (Fig. 5d) from 4.0 mm (for PPCP-0.2) to 0.41 mm (for PPCP-4.6), which suggest less thick sample may also be sufficient to provide a desired level of attenuation.

It is well established that under good conductor approximation, theoretical SE_R and SE_A values follow logarithmic and square root conductivity dependence as per following expressions [48–50]:

$$SE_R\ (dB) = -10\log_{10}\left(\frac{\sigma_T}{16\omega\varepsilon'\varepsilon_o\mu'}\right) \quad (5)$$

$$SE_A\ (dB) = -20\frac{t}{\delta}\log_{10} e = -8.68\left(\frac{t}{\delta}\right) = -8.68t\left(\frac{\sigma_T\omega\mu_r}{2}\right)^{\frac{1}{2}} \quad (6)$$

Therefore, we have plotted SE_R versus $\log(\sigma)$ (Fig. 6a) and SE_A versus $(\sigma)^{1/2}$ (Fig. 6b) graphs at a frequency of 12.4 GHz. It can be clearly seen that, linear dependence of SE_R on $\log(\sigma)$ is applicable only at low MWCNT loading samples (up to 0.9%). In contrast, SE_A versus $(\sigma)^{1/2}$ linearity is valid only for higher loading samples. These results revealed that for a given sample thickness, SE of higher MWCNT loading samples receives major contribution from SE_A (e.g. for PPCP-4.6, $SE_R \sim -5.4$ dB & $SE_A \sim -42.5$ dB) compared to SE_R. Another important parameter for comparing the shielding performance is specific shielding effectiveness (SSE) i.e. SE per unit density of the material [1,21,48]. Generally filled NCs display low value of SSE and foaming is employed to reduce the density and to improve the SSE value. Interestingly, PPCP is low cost and low density material (even in the absence of foaming), which is an important consideration in terms of commercial viability of these NCs. It is worth noting that these PPCP-4.6 with density of 0.94 g/cm^3 and attenuation level of −47.88 dB (that corresponds to blocking of more than 99.99% of the incident EM radiation), display SSE value of ~−51 dB cm^3/g, which is much better than copper (SSE~−10 dB cm^3/g) and many foamed NCs or carbon based foams [51,52]. These finding are of particular interest from the viewpoint of economic aspects and weight consideration, which are of paramount importance for designing a shielding material for high-tech areas like defence, space or medicine.

3.5. *Mechanical properties*

Nano reinforcements tend to cluster together (due to the strong Van der Waal forces), especially under high loading conditions, which result in failure to translate their nanoscopic properties into filled polymer matrix NCs. The improved dispersion & de-agglomeration of fillers and load bearing interface are the keys for development of structurally strong composites, especially at high filler loadings where acceptable, EMI shielding performances are observed. Therefore, we have measured the mechanical properties

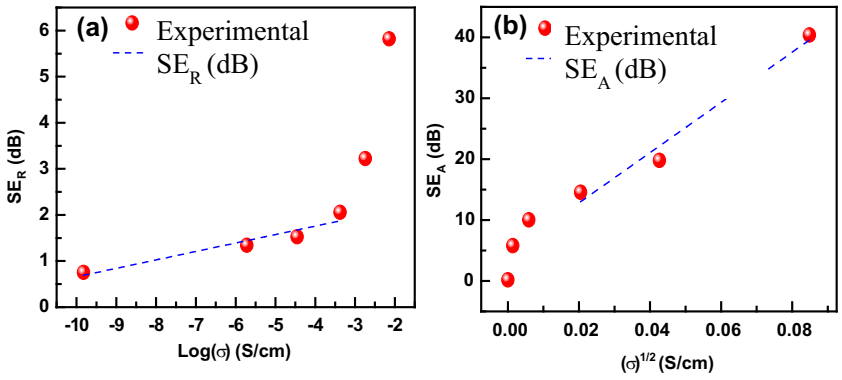

Fig. 6 – Conductivity dependence of (a) SE_R and (b) SE_A, showing logarithmic and square root dependence respectively. (A color version of this figure can be viewed online.)

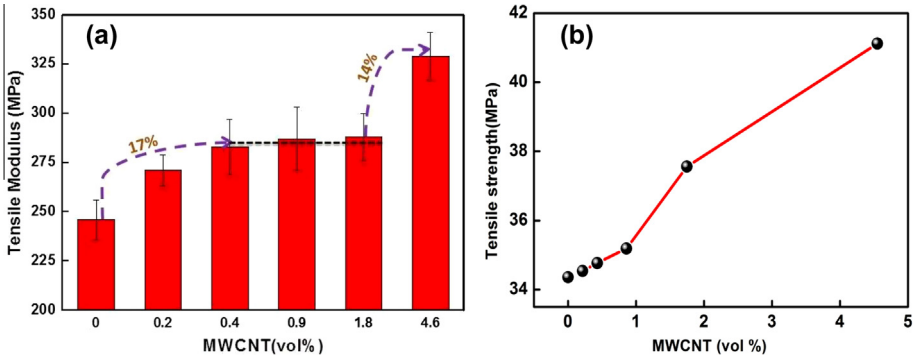

Fig. 7 – Variation of (a) tensile modulus and (b) tensile strength of PPCP/MWCNT composites as a function of MWCNT content. (A color version of this figure can be viewed online.)

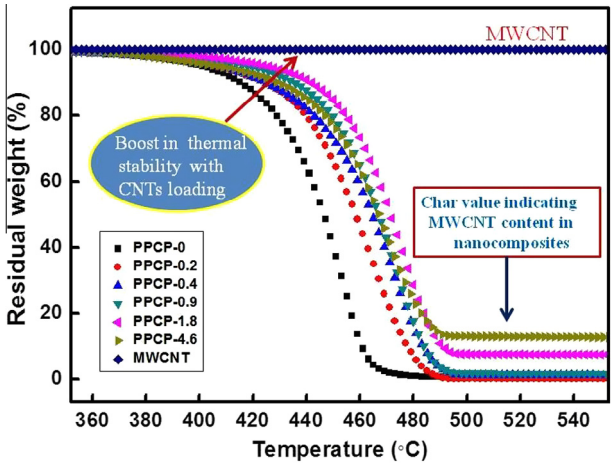

Fig. 8 – TGA traces of MWCNT, PPCP and PPCP/MWCNT composites. (A color version of this figure can be viewed online.)

(strength and modulus) to ensure the absence of any mechanical strength deterioration of composites (generally occur due to agglomeration at such high loadings) and occurrence of reinforcement effect.

Fig. 7a and b shows the variation of tensile strength, and tensile modulus as a function of MWCNT content. It is observed that incorporation of MWCNTs leads to 23% improvement in tensile strength (Fig. 7a) i.e. 34 MPa (for PPCP-0) to 42 MPa (for PPCP-4.6). This reinforcing action may be attributed to the homogenous dispersion of MWCNTs and interfacial adhesion that are essential for the load transfer to MWCNTs across the CNT-matrix interface. Further, MWCNTs have been shown to improve the crystallization of PPCP matrix [53] that may also contribute toward reinforcement and stiffening. Indeed it was also observed that, with the incorporation of 1.8 and 4.6 vol% MWCNTs, the elastic modulus of PPCP (Fig. 7b) increased by ~17% and 34%, respectively. Thus MWCNTs are able to impart stiffness and strength to the polymer matrix which is considered beneficial from the viewpoint of practical applicability, particularly for realizing structurally strong EMI shielding NCs.

3.6. *Thermal analysis by TGA*

As the shields are often exposed to elevated temperature conditions during service life, we have performed (TGA) to assess the thermal stability of the NCs. Fig. 8 displays the TG traces of PPCP and its MWCNT based NCs.

It can be seen that PPCP as well as PPCP/MWCNT NCs display single step degradation. The thermal stability was compared on the basis of initial degradation temperature (IDT), temperature at the maximum mass loss rate (T_{max}) and final degradation temperature (FDT). All these temperatures showed an increase with increasing amounts of MWCNTs. Particularly, an increase of ~12 and ~18 °C was observed in samples having 1.8 and 4.6 vol% MWCNTs respectively (Table 1). This could be attributed to the higher thermal conductivity of CNTs that facilitates heat dissipation within the NCs, thereby preventing or retarding the local accumulation of heat and consequent degradation which may be responsible for an increase in IDT, FDT and T_{max}. It can be seen that MWCNTs did not show any mass loss up to 500 °C whereas PPCP loses more than 99.82% at 500 °C (i.e. char yield

Table 1 – Results of TG/DTG traces PPCP and PPCP/MWCNT NCs (heating rate 20 °C/min, N_2 atm).

Sample designation	% CNT	IDT (°C)	T_{max} (°C)	FDT (°C)	% char at 700 (°C)
PPCP-0	0	436	464	480	0.189
PPCP-0.2	0.5	445	472	484	0.89
PPCP-0.4	1	446	472	484	1.06
PPCP-0.9	2	447	474	484	2.29
PPCP-1.8	4	448	475	488	4.17
PPCP-4.6	10	454	480	490	11.73

of 0.18%); therefore, like for other systems, char residue can be used to determine the filler (here MWCNTs) content.

The results (Table 1) show that with increase in MWCNT loading char residue increases from 0.189% (for PPCP-0) to 11.73% (PPCP-4.6), which is in good agreement with actually loaded CNT content. Overall, the better thermal stability of these NCs (>350 °C) ensures their practical utility.

4. Conclusions

Mechanically strong and thermally stable EMI shielding MWCNT/PPCP NCs containing up to 4.6 vol% have been successfully prepared by commercially viable technique, using melt recirculation equipped twin screw extruder. These NCs display very low percolation threshold (0.19 vol%) which is the indication of good dispersion of MWCNTs within the PPCP matrix. The morphological (SEM/TEM images), spectroscopic (Raman) and electrical (conductivity) measurements have confirmed the good CNT dispersion within PPCP matrix and interaction between the phases. The NC having 4.6 vol% CNT loading (PPCP-4.6) display EMI SE of ~ −48 dB (>99.99% attenuation) along with good thermal stability (>350 °C) and satisfactory mechanical properties (strength ~ 41 MPa and modulus ~ 329 MPa), that justify their suitability for making lightweight, structurally strong and thermally stable EMI shielding material for techno-commercial applications. In addition, these NCs also display specific SE value of ~51 dB cm^3/g, which is highest among unfoamed filled polymer NCs. These studies lay the foundations for the development of commercially viable EMI shielding materials.

Acknowledgments

The authors would like to thank Director CSIR-National Physical Laboratory (NPL), New Delhi, India for extending MWCNTs synthesis and melt processing facilities and Ministry of Human Resource Development (MHRD), India for providing financial assistance to one of the author (Mr. Pawan Verma).

REFERENCES

[1] Saini P. Electrical properties and electromagnetic interference shielding response of electrically conducting thermosetting nanocomposites. Thermoset nanocomposites. Wiley-VCH Verlag GmbH & Co. KGaA; 2013. p. 211–37.
[2] Yang Y, Gupta MC, Dudley KL, Lawrence RW. A comparative study of EMI shielding properties of carbon nanofiber and multi-walled carbon nanotube filled polymer composites. J Nanosci Nanotechnol 2005;5(6):927–31.
[3] Saini P, Arora M, Gupta G, Gupta BK, Singh VN, Choudhary V. High permittivity polyaniline–barium titanate nanocomposites with excellent electromagnetic interference shielding response. Nanoscale 2013;5(10):4330–6.
[4] Chung DDL. Electromagnetic interference shielding effectiveness of carbon materials. Carbon 2001;39(2):279–85.
[5] Chung DDL. Materials for electromagnetic interference shielding. J Mater Eng Perform 2000;9(3):350–4.
[6] Chung DDL. Electrical applications of carbon materials. J Mater Sci 2004;39(8):2645–61.
[7] Gupta A, Choudhary V. Electrical conductivity and shielding effectiveness of poly(trimethylene terephthalate)/multiwalled carbon nanotube composites. J Mater Sci 2011;46(19):6416–23.
[8] Shui X, Chung DDL. Submicron diameter nickel filaments and their polymer-matrix composites. J Mater Sci 2000;35(7):1773–85.
[9] Wen S, Chung DDL. Electromagnetic interference shielding reaching 70 dB in steel fiber cement. Cem Concr Res 2004;34(2):329–32.
[10] Luo X, Chung DDL. Electromagnetic interference shielding reaching 130 dB using flexible graphite. Carbon 1996;34(10):1293–4.
[11] Wang Y, Jing X. Intrinsically conducting polymers for electromagnetic interference shielding. Polym Adv Technol 2005;16(4):344–51.
[12] Li N, Huang Y, Du F, He X, Lin X, Gao H, et al. Electromagnetic interference (EMI) shielding of single-walled carbon nanotube epoxy composites. Nano Lett 2006;6(6):1141–5.
[13] Ma C-CM, Huang Y-L, Kuan H-C, Chiu Y-S. Preparation and electromagnetic interference shielding characteristics of novel carbon-nanotube/siloxane/poly-(urea urethane) nanocomposites. J Polym Sci B Polym Phys 2005;43(4):345–58.
[14] Gupta A, Choudhary V. Electromagnetic interference shielding behavior of poly(trimethylene terephthalate)/multi-walled carbon nanotube composites. Compos Sci Technol 2011;71(13):1563–8.
[15] Gupta A, Choudhary V. Effect of multiwall carbon nanotubes on thermomechanical and electrical properties of poly(trimethylene terephthalate). J Appl Polym Sci 2012; 123(3):1548–56.
[16] Yang Y, Gupta MC, Dudley KL, Lawrence RW. Novel carbon nanotube–polystyrene foam composites for electromagnetic interference shielding. Nano Lett 2005;5(11):2131–4.
[17] Huang Y-L, Yuen S-M, Ma C-CM, Chuang C-Y, Yu K-C, Teng C-C, et al. Morphological, electrical, electromagnetic interference (EMI) shielding, and tribological properties of functionalized multi-walled carbon nanotube/poly methyl methacrylate (PMMA) composites. Compos Sci Technol 2009;69(11–12):1991–6.
[18] Liu Z, Bai G, Huang Y, Ma Y, Du F, Li F, et al. Reflection and absorption contributions to the electromagnetic interference shielding of single-walled carbon nanotube/polyurethane composites. Carbon 2007;45(4):821–7.
[19] Huang Y, Li N, Ma Y, Du F, Li F, He X, et al. Carbon 2007;45(8):1614.
[20] Saini P, Choudhary V, Singh BP, Mathur RB, Dhawan SK. Enhanced microwave absorption behavior of polyaniline-CNT/polystyrene blend in 12.4–18.0 GHz range. Synth Met 2011;161(15–16):1522–6.
[21] Saini P, Choudhary V. Enhanced electromagnetic interference shielding effectiveness of polyaniline functionalized carbon nanotubes filled polystyrene composites. J Nanopart Res 2013;15(1):1–7. http://dx.doi.org/10.1007/s11051-012-1415-2.
[22] Ajayan PM, Stephan O, Colliex C, Trauth D. Aligned carbon nanotube arrays formed by cutting a polymer resin—nanotube composite. Science 1994;265(5176):1212–4.
[23] Thostenson ET, Li C, Chou TW. Nanocomposites in context. Compos Sci Technol 2005;65(3–4):491–516.
[24] Alexandre M, Dubois P. Polymer-layered silicate nanocomposites: preparation, properties and uses of a new class of materials. Mater Sci Eng R 2000;28(1–2):1–63.
[25] Kum C, Sung Y-T, Han M, Kim W, Lee H, Lee S-J, et al. Effects of morphology on the electrical and mechanical properties of the polycarbonate/multi-walled carbon nanotube composites. Macromol Res 2006;14(4):456–60.

[26] Kim M-S, Yan J, Joo K-H, Pandey JK, Kang Y-J, Ahn S-H. Synergistic effects of carbon nanotubes and exfoliated graphite nanoplatelets for electromagnetic interference shielding and soundproofing. J Appl Polym Sci 2013;130(6):3947–51.
[27] Al-Saleh MH, Sundararaj U. Electromagnetic interference shielding mechanisms of CNT/polymer composites. Carbon 2009;47(7):1738–46.
[28] Park D, Lee Y, Park S, Lee C, Kim S, Kim W. Effects of hybrid fillers on the electrical conductivity and EMI shielding efficiency of polypropylene/conductive filler composites. Macromol Res 2013;21(8):905–10.
[29] Thomassin J-M, Huynen I, Jerome R, Detrembleur C. Functionalized polypropylenes as efficient dispersing agents for carbon nanotubes in a polypropylene matrix; application to electromagnetic interference (EMI) absorber materials. Polymer 2010;51(1):115–21.
[30] Arjmand M, Mahmoodi M, Gelves GA, Park S, Sundararaj U. Electrical and electromagnetic interference shielding properties of flow-induced oriented carbon nanotubes in polycarbonate. Carbon 2011;49(11):3430–40.
[31] Villmow T, Pötschke P, Pegel S, Häussler L, Kretzschmar B. Influence of twin-screw extrusion conditions on the dispersion of multi-walled carbon nanotubes in a poly(lactic acid) matrix. Polymer 2008;49(16):3500–9.
[32] Pötschke P, Bhattacharyya AR, Janke A. Carbon nanotube-filled polycarbonate composites produced by melt mixing and their use in blends with polyethylene. Carbon 2004;42(5–6):965–9.
[33] Mathur RB, Chatterjee S, Singh BP. Growth of carbon nanotubes on carbon fibre substrates to produce hybrid/phenolic composites with improved mechanical properties. Compos Sci Technol 2008;68(7–8):1608–15.
[34] Kim HM, Kim K, Lee CY, Joo J, Cho SJ, Yoon HS, et al. Electrical conductivity and electromagnetic interference shielding of multiwalled carbon nanotube composites containing Fe catalyst. Appl Phys Lett 2004;84(4):589–91.
[35] Kum C, Sung Y-T, Han M, Kim W, Lee H, Lee S-J, et al. Effects of morphology on the electrical and mechanical properties of the polycarbonate/multi-walled carbon nanotube composites. Macromol Res 2006;14(4):456–60.
[36] Chipara DM, Macossay J, Ybarra AV, Chipara A, Eubanks TM, Chipara M. Raman spectroscopy of polystyrene nanofibers—multiwalled carbon nanotubes composites. Appl Surf Sci 2013;275:23–7.
[37] Ram R, Rahaman M, Khastgir D. Electrical properties of polyvinylidene fluoride (PVDF)/multi-walled carbon nanotube (MWCNT) semi-transparent composites: modelling of DC conductivity. Compos A 2015;69:30–9.
[38] Kim HM, Kim K, Lee SJ, Joo J, Yoon HS, Cho SJ, et al. Charge transport properties of composites of multiwalled carbon nanotube with metal catalyst and polymer: application to electromagnetic interference shielding. Curr Appl Phys 2004;4(6):577–80.
[39] Liang J, Wang Y, Huang Y, Ma Y, Liu Z, Cai J, et al. Electromagnetic interference shielding of graphene/epoxy composites. Carbon 2009;47(3):922–5.
[40] Li Y, Chen C, Zhang S, Ni Y, Huang J. Electrical conductivity and electromagnetic interference shielding characteristics of multiwalled carbon nanotube filled polyacrylate composite films. Appl Surf Sci 2008;254(18):5766–71.
[41] Obukhov SP. First order rigidity transition in random rod networks. Phys Rev Lett 1995;74(22):4472–5.
[42] Regev O, ElKati PNB, Loos J, Koning CE. Preparation of conductive nanotube–polymer composites using latex technology. Adv Mater 2004;16(3):248–51.
[43] Ounaies Z, Park C, Wise KE, Siochi EJ, Harrison JS. Electrical properties of single wall carbon nanotube reinforced polyimide composites. Compos Sci Technol 2003;63(11):1637–46.
[44] Sandler JKW, Kirk JE, Kinloch IA, Shaffer MSP, Windle AH. Ultra-low electrical percolation threshold in carbon-nanotube-epoxy composites. Polymer 2003;44(19):5893–9.
[45] Saini P, Choudhary V, Singh BP, Mathur RB, Dhawan SK. Polyaniline–MWCNT nanocomposites for microwave absorption and EMI shielding. Mater Chem Phys 2009;113(2–3):919–26.
[46] Hu G, Zhao C, Zhang S, Yang M, Wang Z. Low percolation thresholds of electrical conductivity and rheology in poly(ethylene terephthalate) through the networks of multi-walled carbon nanotubes. Polymer 2006;47(1):480–8.
[47] Ott HW. Electromagnetic compatibility. Electromagnetic compatibility engineering. John Wiley & Sons, Inc.; 2009. p. 1–43.
[48] Saini P, Choudhary V, Vijayan N, Kotnala R. Improved electromagnetic interference shielding response of poly (aniline)-coated fabrics containing dielectric and magnetic nanoparticles. J Phys Chem C 2012;116(24):13403–12.
[49] Yang Y, Gupta MC, Dudley KL, Lawrence RW. Conductive carbon nanofiber–polymer foam structures. Adv Mater 2005;17(16):1999–2003.
[50] Hong YK, Lee CY, Jeong CK, Lee DE, Kim K, Joo J. Method and apparatus to measure electromagnetic interference shielding efficiency and its shielding characteristics in broadband frequency ranges. Rev Sci Instr 2003;74(2):1098–102.
[51] Zhang H-B, Yan Q, Zheng W-G, He Z, Yu Z-Z. Tough graphene–polymer microcellular foams for electromagnetic interference shielding. ACS Appl Mater Interfaces 2011;3(3):918–24.
[52] Zhang Y, Huang Y, Zhang T, Chang H, Xiao P, Chen H, et al. Broadband and tunable high-performance microwave absorption of an ultralight and highly compressible graphene foam. Adv Mater 2015. http://dx.doi.org/10.1002/adma.20140578.
[53] Verma P, Choudhary V. Polypropylene random copolymer/MWCNT nanocomposites: isothermal crystallization kinetics, structural, and morphological interpretations. J Appl Polym Sci 2015;132(13).